minerals

MDPI

Article

Mineralogical and Geochemical Characteristics of Carbonates and Their Geological Significance to the Fuli Pb-Zn Deposit, Yunnan Province

Xingyu Liang [1], Bo Li [1,*], Chengnan Zhang [2], Huaikun Qin [3], Gao Li [3] and Xinyue Zhang [4]

[1] Faculty of Land Resources Engineering, Kunming University of Science and Technology, Kunming 650093, China
[2] Yunnan Tin Industry Group (Holding) Company Limted R & D Center, Kunming 650200, China
[3] Fuli Lead-Zinc Mine Co., Ltd., Fuyuan 655504, China
[4] Kunming Geological Prospecting Institute, China Metallurgical Geological Bureau, Kunming 650024, China
* Correspondence: libo1964@sina.com

Abstract: Mississippi Valley-Type (MVT) deposits are among the main types of Pb-Zn deposits that feature carbonate minerals as the main gangue minerals; their formation runs through the entire metallogenic process of MVT deposits. Therefore, carbonate minerals contain rich information on metallogenic fluid evolution and are thus important prospecting indicators. The Fuli Pb-Zn deposit in eastern Yunnan is located in the southeast of the Sichuan-Yunnan-Guizhou (SYG) Pb-Zn metallogenic province, which is the biggest producer of zinc and lead in China and contains more than 400 deposits and over 20 million tons of Pb + Zn reserves. The ore occurs in the interlayer fracture zone of Middle Permian Yangxin Formation Dolomite, and the orebody shape is generally stratiform. The main metal-bearing minerals of this deposit are sphalerite, galena, and pyrite; the gangue minerals mainly comprise dolomite and calcite. Three mineralized stages are observed (the early metallogenic period, the main metallogenic period, and the late metallogenic period) according to the characteristics of stratigraphic output, the intercalated contact relationship of gangue minerals, and the alteration characteristics of the wall rock. To determine the source and properties of the ore-forming fluid and the ore-forming process of the Fuli Pb-Zn deposit, different stages of mineralogy and trace element geochemical characteristics of hydrothermal dolomite were systematically studied. The minerals were observed under microscope and subjected to in situ analysis by LA-ICP-MS and C–O isotope test. The $\delta^{18}O_{SMOW}$ value of the dolomite in the metallogenic period was between 13.29‰ and 20.55‰, and the $\delta^{13}C_{PDB}$ value was between −4.13‰ and 3.5‰. Dolomite of the metallogenic period mainly came from the dissolution of carbonate wall rocks, while C in the ore-forming fluid came from the wall rocks. A few dolomites showed a trend of depleting $\delta^{13}C_{PDB}$ and $\delta^{18}O_{SMOW}$ at the same time, implying the influence of sedimentary rock contamination in the mantle multiphase system. The lower $\delta^{18}O$ was due to the exchange of O isotopes between the wall rocks and the depleted $\delta^{18}O$ in ore-forming fluids. From the early to the later stage of mineralization, the ore-forming fluid changed from alkaline to neutral to weakly acidic due to a decrease in the oxygen fugacity and temperature of the fluid; this change resulted in the precipitation of sulfide and dolomite in the deposit. From the early to the late stages of mineralization, Fe and Mn showed a downward trend. Fe and Mn entered the alkaline environment of the carbonate minerals, while Fe and Mn were released into the acidic fluid, indicating that due to the metasomatism from strong to weak, their metallogenic environment evolved from alkaline to acidic. From the early to the late stage of mineralization, Sr showed an upward trend, which might indicate that the continuous reaction between the hydrothermal fluid and the wall rock continuously released Sr into the fluid. The Fe-Sr and Mn-Sr diagrams show that two kinds of fluid mixing occurred in the ore-forming process. The Fuli Pb-Zn deposit may have formed from mineral precipitation caused by the mixing of the metal-rich, oxidized acidic fluid and the sulfur-rich, reduced alkaline fluid. The results show that the Fuli Pb-Zn deposit belongs to MVT deposits.

Citation: Liang, X.; Li, B.; Zhang, C.; Qin, H.; Li, G.; Zhang, X. Mineralogical and Geochemical Characteristics of Carbonates and Their Geological Significance to the Fuli Pb-Zn Deposit, Yunnan Province. *Minerals* **2022**, *12*, 1317. https://doi.org/10.3390/min12101317

Academic Editors: Callum Hetherington and Maria Boni

Received: 1 July 2022
Accepted: 29 September 2022
Published: 19 October 2022

Keywords: LA-MC-ICPMS; C-O isotope; source of metallogenic material; Fuli Pb-Zn deposit; Sichuan-Yunnan-Guizhou Pb-Zn metallogenic province

1. Introduction

The Sichuan-Yunnan-Guizhou (SYG) metallogenic province is located on the southwestern margin of the Yangtze craton in South China. It hosts world-class concentrations of lead (Pb), zinc (Zn), silver (Ag), and germanium (Ge) deposits, which are mostly associated with low-temperature fluids (<300 °C) [1–6]. The Pb-Zn deposits in this area mainly occur in a range of carbonate rocks from the Neoproterozoic Sinian Dengying Formation to the Late Paleozoic Permian Yangxin Formation. These deposits are characterized by high Pb and Zn grades and are enriched in Cd, Ge, Ga, etc. Mineralization, which is generally structurally controlled by faults and folds, is interpreted as epigenetic [7] and controlled by the fault-fold structural system. Previous studies generally agree on its nature as an epigenetic deposit [8–16].

The Fuli Pb-Zn deposit is located in the southeast of the Sichuan-Yunnan-Guizhou Pb-Zn ore concentration area in Fuyuan County, Yunnan Province (Figure 1). The deposit occurs in the interlayer fractured zone of Middle Permian Yangxin Formation Dolomite, and the orebody shape is stratiform. Studies and reports on this deposit are rare, particularly those focused on carbonate minerals. Carbonate minerals are gangue minerals in many deposits and are especially important in Mississippi Valley-Type (MVT) deposits [17]. Carbonate minerals run through the entire metallogenic process of MVT deposits. Therefore, carbonate minerals carry rich metallogenic information that is important for understanding the genesis of MVT deposits. Compared to traditional methods for trace element analysis, LA-ICP MS (laser ablation-inductively coupled plasma mass spectrometry) is an in situ analysis method that can overcome the problem of sample contamination caused by sample selection and effectively judge the spatial distributions of trace elements in the sample [18,19].

In this article, with the help of LA multi-collector ICP MS (LA-MC-ICP MS), we performed a detailed mineralogical and in situ trace element composition study on gangue minerals (dolomite and calcite) from the Fuli Pb-Zn deposit. The composition and distribution characteristics of trace elements in the gangue minerals of the ore deposit and their geological significance were investigated to determine the source and properties of the ore-forming fluid forming this deposit.

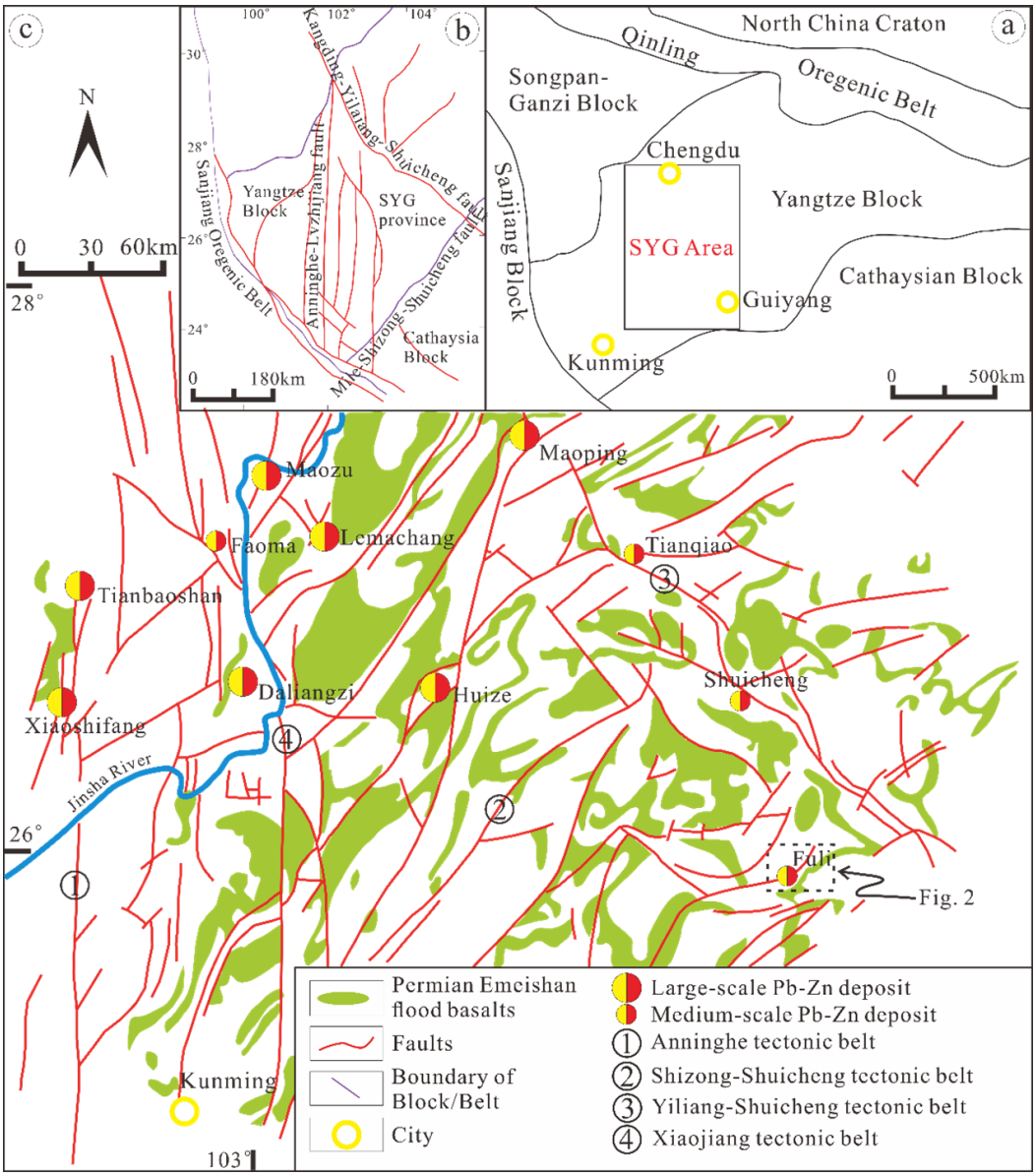

Figure 1. (**a**) Simplified geological framework of SW China showing the SYG province. (**b**) Regional geological setting of SW China. (**c**) A sketched geological map of the SYG metallogenic province showing the distribution of Pb-Zn deposits and Emeishan Flood basalt and location of the Fuli deposit (modified from [3,6,20]).

2. Geological Setting of the Region and Deposit

2.1. Tectonic Features

The study area is located between the Qujing and Mile-Shizong faults (Figure 1). The exposed basement of the study area is the Kunyang Group of the Meso-Neo Proterozoic era, while the Sinian, Cambrian, Ordovician, and Silurian are missing above the Kunyang Group. The Haikou Formation of the Middle Devonian is in direct contact with the Kunyang Group in an angular unconformity, and the Kunyang Group is only exposed in the southwest of the study area. The Proterozoic structure framework is dominated by the east-west trend. After the Jinning, Caledonian, and Hercynian movements, the structure in the area was transformed into a north-south-trending structure supplemented by a north-east-trending structure, both north-west and east-west structures inherited. During the Yanshan and Himalayan tectonic movements, the northwest-trending structure was dominantly active and gradually formed the current north-south-trending structure followed by the north-east-

trending structure. The east-west and northwest-trending structures were also developed at this time. In general, carbonate and clastic rocks of the Proterozoic and Paleozoic eras were deposited in the platform fold belt with a total thickness of more than 10,000 m. They show the characteristics of long-term depression deposition in this area. The strata in the Sinian to Permian eras are relatively well developed but exhibit frequent discontinuities. The late Hercynian period witnessed the large-scale eruption of basalt magma and its intrusion; thus, it is the only magmatic rock in the area. The structural framework is characterized by parallel and almost equidistant north-south-trending faults. The northeast-trending structures are also relatively clear with large scale and a long developmental history. The north-south- and northwest-trending structures play important roles in controlling the formation, distribution, and enrichment of Zn-Pb deposits in the region.

The Mile-Shizong fault is the main fault in the region. The Tuoniu-Duza anticline on the west side of the mining area is the most important fold structure in the region (Figure 1b). Together, both the fault and the anticline control the distribution of regional strata along with the distribution of secondary structures and mineralization in the area. The Mile-Shizong fault is generally northeast trending (north-northeast trending near the mining area). The fault zone is composed of multiple high-angle and steep faults, and the faults are generally compressional reverse faults. The Tuoniu-Duza anticline is a gentle structure with a stratum dip angle of 10–12° on both flanks and a north-northeast-trending axis, consistent with the Mile-Shizong fault.

This area experienced a near-SN-trending extension in the Late Permian. During the Late Triassic, it was affected by tectonic events such as the collisional orogeny of the Indosinian and South China Plates and the Yidun arc collisional orogen, forming a series of near SN-NNE compressive torsional fractures (Figure 2a). Influenced by the Late Triassic compressional structure and the Tuoniu-Duza anticline, a series of extensional fissures and interlayer fracture zones were generated in the middle Yangxin Formation (P_2y^2), which provided structural traps for circulating metal-rich fluids. The NE-NNE-trending structures developed in the mining area (Figure 2a) are post-metallogenic structures with dip angles of 50–80°. These structures have deformed and modified the continuity of the mineral body.

2.2. Deposit Geology

The Fuli Pb-Zn deposit is located in the southeastern section of the SYG metallogenic province in the southwestern margin of the Yangtze craton. The Early-Middle Permian era, which was the largest transgressive cycle in this area during the Late Paleozoic, mainly led to the formation of carbonate deposits. Under the influence of continental uplift, a set of neritic Mg-bearing carbonate assemblages was developed. The strata of the Middle Permian Yangxin Formation (P_2y) are exposed in the mining area (Figure 2b), and the lithology of the lower section (P_2y^1) is light-grey limestone with dolomite. The middle section (P_2y^2) is mainly interbedded with light-grey limestone and dolomite with local siliceous dolomite; it is the main type of stratum occurring in the Pb-Zn polymetallic deposits. The upper section (P_2y^3) is grey medium-thick layered crystalline limestone with a small amount of dolomitic limestone and dolomite containing flint bands. The Pb-Zn ore in the mining area is hosted in dolomitic limestone, and the shape of the orebodies is stratiform. At present, two Pb-Zn mineralization bodies have been found in the Fuli Pb-Zn mine.

Mineral body #1: This mineral body is 210 m in length with an inclination extension of 314 m, true thickness of 1.11 m, overall inclination of 181°, and dip angle of 15°. The body is distributed in the southern part of the mining area. The average grades of Pb and Zn are 1.51% and 8.43%, respectively. The mineral body is thick in the middle and thin at both ends. In addition, the surface is thin and low grade, while the body becomes thicker and the metal grade increases with greater depth.

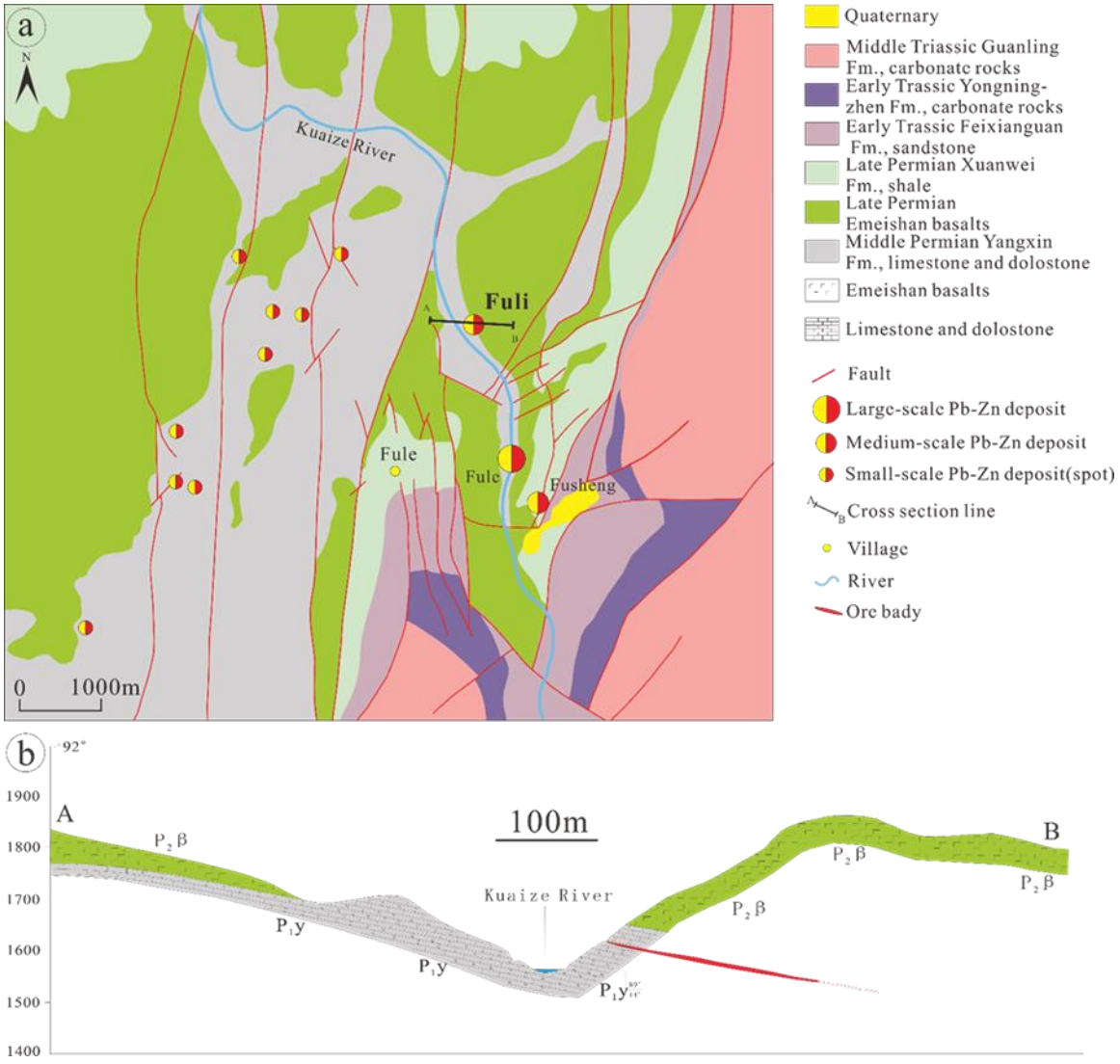

Figure 2. (**a**) Geological sketch map of the Fuli Pb−Zn deposit (modified after [6] Zhou et al., 2018). (**b**) A-B Cross-section of the Fuli deposit.

Mineral body #II: The mineral body is distributed in the northern part of the mining area with an unexposed surface. The mineral body features a layered output with a 220-m-long engineering control trend, an inclination extension of 103–215 m, an overall inclination of 144°, and a dip angle of 12°. The thickness of the mineral body is 1.00–1.20 m, with an average of 1.11 m. The average grades of Pb and Zn are 5.20% and 13.29%, respectively. Characteristically, the mineral body is thick in the middle, where the mineral grade is high, and thin at both ends, where the mineral grade is low. In the hanging wall of the normal fault, the mineral body shows thickening and enrichment.

Through field surveys, observations of ore texture and mineral association, and previous petrographic work, the formation process of the Fuli Pb-Zn deposit was divided into three stages: the early metallogenic period, main metallogenic period, and late metallogenic period (Figures 3 and 4).

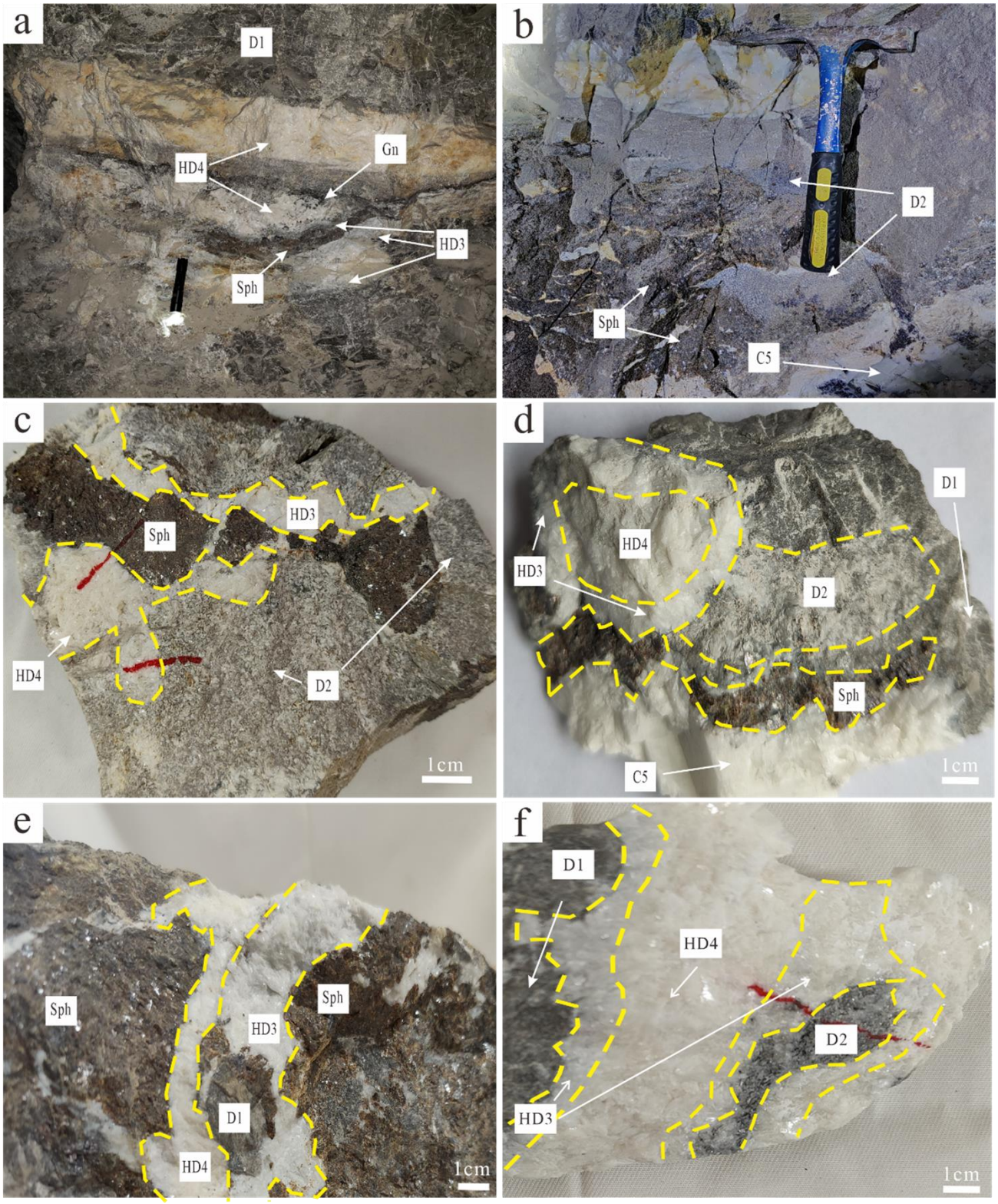

Figure 3. Photographs of samples from the Fuli Pb-Zn deposit. (**a**,**b**) Massive Sp and/or Gn are filled/cemented by Dol/Cal veins. (**c**) D2 altered dolostone disseminated by sphalerite and galena and HD3 grey dolomite coexisting with sphalerite and galena. (**d**) Hydrothermal dolomite cement host rock and sphalerite clasts, both cut by late calcite. (**e**) Dark and red-brown sphalerite and HD3 grey dolomite crosscut by HD4 white dolomite. (**f**) HD4 white dolomite replacing HD3 grey dolomite.

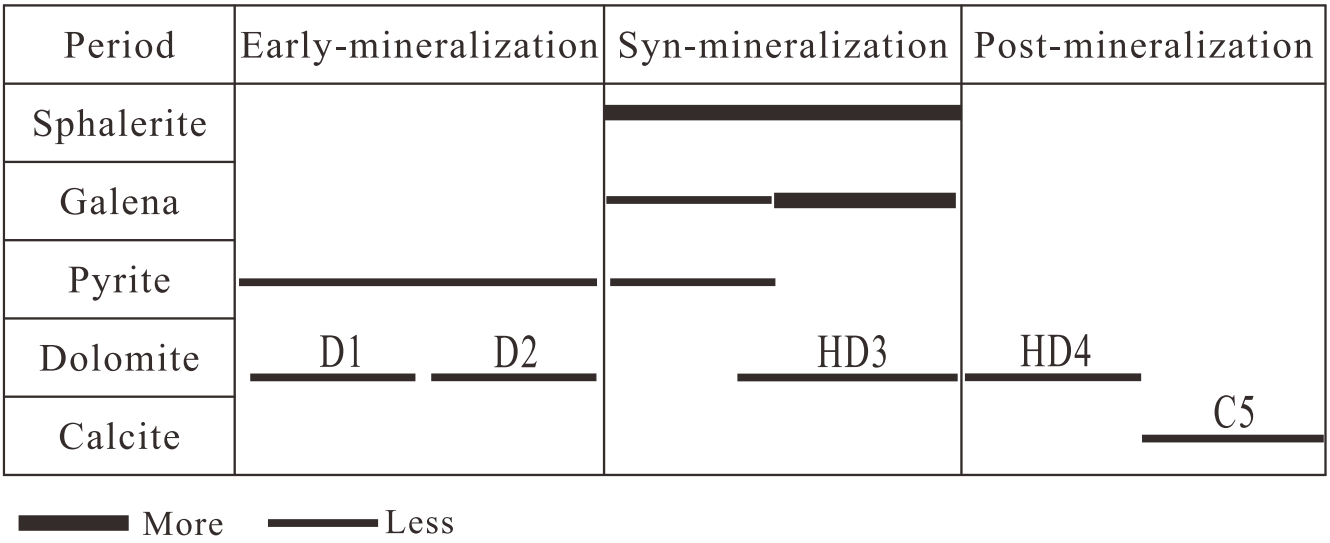

Figure 4. Mineral paragenesis in the Fuli Pb-Zn deposit.

Early metallogenic period: The main feature of the ore, which was formed in the early metallogenic period, is hydrothermal alteration dolomitization. The dolomite formed during this period can be divided into two stages: the D1 and D2 stages. The D1 dolomite appears as grey-black, fine-grained xenomorphic granules. (Figure 3f) Sphalerite and galena are mostly found in the D1 breccia gap of the dolomite. This kind of dolomite is non-luminescent or presents a dark crimson luminescence under cathodoluminescence (CL). The D1 dolomite is often cemented by ore-forming grey dolomite (Figure 3d). The D2 dolomite is composed of a euhedral white core and a dark grey-grey edge with a coarse grain size of approximately 2 mm and high porosity. This kind of dolomite presents dark red luminescence under CL. The sphalerite and galena are spotted as massive portions or disseminated in the dolomite (Figure 3c).

Main metallogenic period: The mineral body formed in the main metallogenic period was developed in the interlayer fissure zone and spread along the stratum in a layered pattern. The main mineral components are sphalerite, galena, and pyrite. The ore minerals are produced in the form of dense blocks with veins and are disseminated. The sulfides generally have granular (Figure 5i), metasomatic (Figure 5d), and colloidal textures, while others may develop massive and disseminated bodies (Figure 3a) or breccia-like (Figure 3b) and vein-like structures (Figure 3c,d). The sphalerite formed at this stage is mainly reddish-brown to brown-black, and the crystals are mainly subhedral to euhedral in shape. The pre-altered dolomite is wrapped in grey-white and grey-black fine-grained mesocrystalline dolomite that coexists with the sphalerite. It is disseminated and speckled. Agglomerated sphalerite grains are distributed in the dolomite. Galena is present in a cubic crystal form. During the main mineralization period, two phases of dolomite can be identified: grey dolomite (HD3) and white dolomite (HD4). These two kinds of dolomite are hydrothermal bright crystalline dolomite types that are closely related to the ore and form a dolomite halo around the mineral body (Figure 3a,b). The HD3 dolomite is a grey-white, meso-coarse-grained semi-autotype dolomite with a grain size between 0.1 and 0.8 mm; it is distributed along the edges of sphalerite and galena (Figure 3c,e). The iron content of this dolomite is high, and it was formed at the same time as the sulfide. The HD4 dolomite usually presents saddle-like, euhedral coarse crystals that are white-milky white in color. The HD4 dolomite fills open spaces or cement fissures. The HD3 dolomite is in direct contact with metasomatic wall rock, while the HD4 dolomite is mostly in contact with the grey dolomite and was formed later than the grey dolomite (Figure 3f). The HD3 dolomite presents bright red luminescence under CL, while white dolomite shows dark red luminescence.

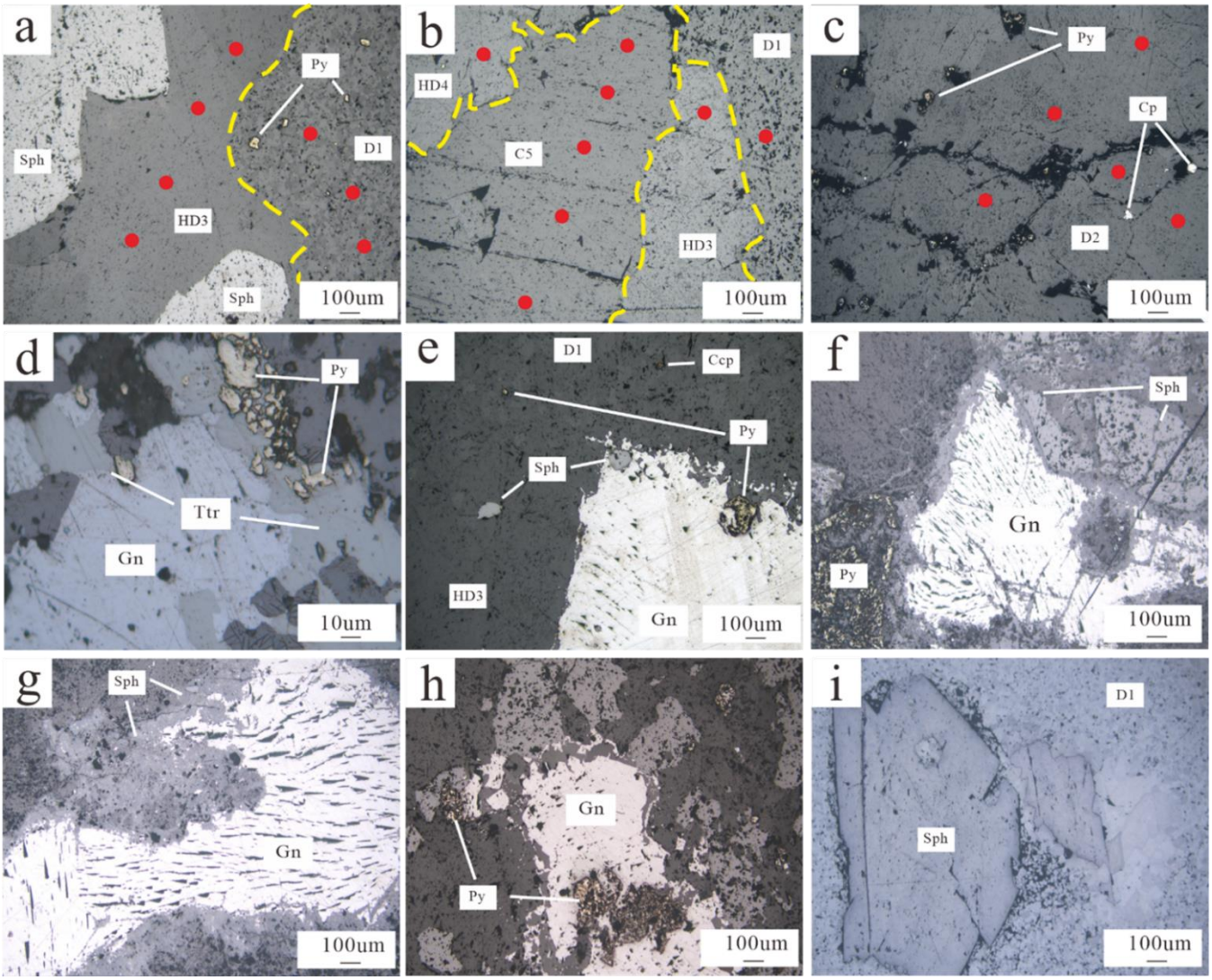

Figure 5. Textural features of minerals from the Fuli Pb-Zn deposit. The red dots represent laser ablation points, and the yellow lines are boundaries between different dolomites. (**a**) HD3 grey dolomite that coexists with sphalerite. (**b**) HD4 white dolomite and HD3 grey dolomite crosscut by euhedral calcite veins. (**c**) Pyrite and chalcopyrite observed as massive portions or disseminated in the D2 dolomite. (**d**,**e**) Galena metasomatic pyrite and/or tetrahedrite. (**f**,**g**) Contacts between sphalerite and galena showing embayment. (**h**) Metasomatic relict pyrite and xenomorphic sphalerite in anhedral sphalerite fracture. (**i**) Dolomite with a granular structure.

Late metallogenic period: The euhedral calcite veins (C5), which are the last stage of gangue minerals, are massively thick veins that enclose the sphalerite and galena formed in the main metallogenic period. This kind of calcite is non-luminescent or presents dark crimson luminescence under CL.

3. Materials and Methods

3.1. Elemental Measurement by LA-ICP MS

In this study, trace element analysis of minerals was conducted by LA-ICP MS at the Wuhan Sample Solution Analytical Technology Co., Ltd., Wuhan, China. The operating conditions for the LA system and the ICP MS instrument and data reduction were the same as those described by Zong et al. [21]. Laser sampling was performed using a Geolas Pro LA system (Coherent Inc., Santa Clara, CA, USA) that consisted of a COMPexPro 102 ArF excimer laser (wavelength of 193 nm and maximum energy of 200 mJ) and a

MicroLas optical system. An Agilent 7900 (Agilent Technologies, Inc., Santa Clara, CA, USA) ICP-MS instrument was used to acquire ion signal intensities. Helium was applied as a carrier gas. Argon was used as the make-up gas and mixed with the carrier gas via a T-connector before entering the ICP instrument. A "wire" signal smoothing device was included in the LA system [22]. The spot size and frequency of the laser were set to 44 μm and 5 Hz, respectively. The trace element compositions of minerals were calibrated against various reference materials (NIST 610, BHVO-2G, BCR-2G, BIR-1G, and MACS-3) without using an internal standard [23,24]. Each analysis incorporated a background acquisition of approximately 20–30 s followed by 50 s of data acquisition from the sample. ICP-MS-DataCal v12.2, an Excel-based software, was used to perform off-line selection and integration of the background; the signals, time-drift correction, and quantitative calibration for trace element analysis [23].

3.2. C-O In Situ Isotopes

Sixteen representative samples were selected, and microdrill sampling was carried out in the proposed area (wall rock, metallogenic area, and non-metallogenic area) for C-O isotopic analysis. The dolomite C–O isotope test and analysis were performed in the Stable Isotope Analysis Laboratory of Kunming University of Science and Technology, China. The test adopted the 100% phosphoric acid method. The sample reacted with phosphoric acid for more than 1 h at 90 °C. Under the protection of high-purity helium, the released CO_2 gas was introduced into an ISO Prime 100 gas-phase stable isotope mass spectrometer (Elementar Analysensysteme GmbH, Langenselbold, Hessian, Germany) for the determination of C and O isotope composition. The experiment used Vienna Pee Dee Belemnite (V-PDB) as the standard, where $\delta^{18}O_{SMOW} = 1.03086 \times \delta^{18}O_{PDB} + 30.86$.

3.3. CL Analysis

CL petrography was performed on a Leica DM2700P binocular petrographic microscope (Leica Microsystems, Wetzlar, Hessian, Germany) with a CLF-2 CL system (BII Inc., Markham, ON, Canada) at the Key Laboratory of Mineralogy and Metallogeny, GIGCAS. The voltage for the systems was held between 13 and 15 kV, the current ranged from 240 to 260 μA, and chamber pressure was between 50 and 60 millitorrs.

4. Results

4.1. CL Images of Dolomite

The CL images for representative dolomite samples are illustrated in Figure 6. The different stages of dolomite exhibited different characteristics under CL. In the early metallogenic period, the D1 dolomite was non-luminescent or presented a dark crimson luminescence, while the D2 dolomite presented a dark red luminescence under CL. In the main metallogenic period, the grey dolomite (HD3) presented bright red luminescence, and the white dolomite (HD4) was dark red. In the late metallogenic period, the euhedral calcite veins (C5) were non-luminescent or presented a dark crimson luminescence.

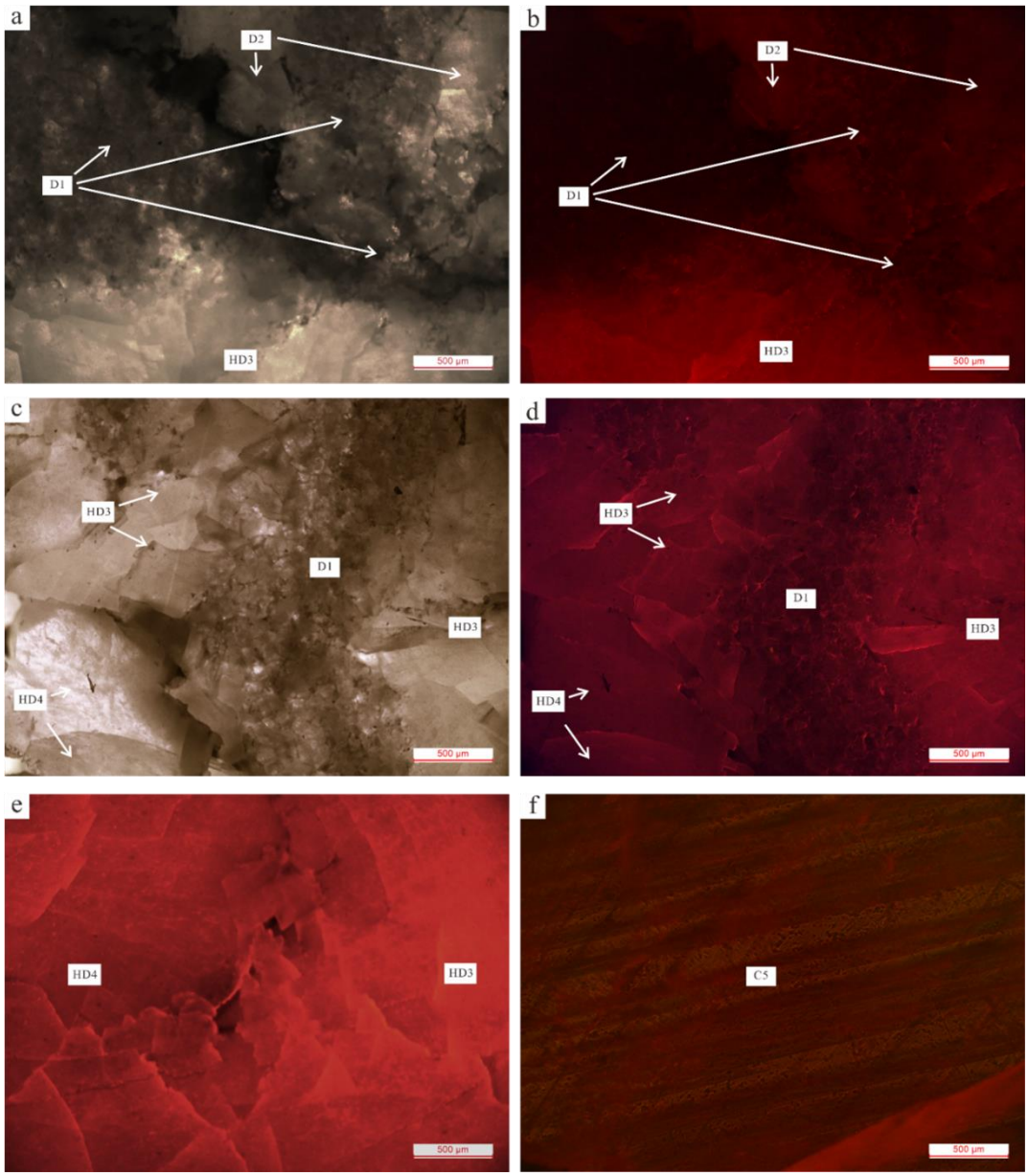

Figure 6. Transmitted light and CL images of carbonate in the Fuli Pb-Zn deposit. (**a**,**b**) D1 dolomite is non-luminescent, D2 dolomite presents dark crimson luminescence under CL, and HD3 grey dolomite presents bright red luminescence under CL. (**c**–**e**) D1 dolomite is non-luminescent under CL, HD3 grey dolomite presents bright red luminescence under CL, and HD4 white dolomite shows dark red luminescence under CL. (**f**) The euhedral calcite veins (C5) are non-luminescent under CL.

4.2. Textural and Mineralogical Analyses

The LA-ICP-MS *in situ* trace element analysis results of carbonate minerals for the Fuli deposits are shown in Table 1, and the variations in these trace elements are shown in Figure 7.

Table 1. Summary of LA-ICP MS carbonate trace element concentration (ppm) in the Fuli Pb-Zn deposit.

Types	Statistics	Na	Al	Si	Mn	Fe	Zn	Sr	Ba	Pb	La	Ce	Pr	Nd	Sm	Eu
D1 (n = 8)	max	516.21	754.03	1504.98	137.45	642.03	53.67	42.34	3.42	21.78	1.61	2.25	0.32	0.94	0.18	0.04
	min	293.14	255.54	721.40	79.68	342.28	4.92	15.58	2.03	0.52	0.35	1.00	0.17	0.44	0.11	0.02
	mean	390.299	499.680	1204.138	110.954	476.725	22.115	26.064	2.653	4.936	1.092	1.365	0.214	0.615	0.131	0.031
D2 (n = 8)	max	302.930	31.590	399.330	110.240	539.230	161.040	16.860	1.100	7.980	3.152	3.412	0.513	1.729	0.304	0.091
	min	108.590	16.650	302.710	98.520	314.170	3.190	7.820	0.040	0.320	0.631	1.067	0.194	0.615	0.135	0.033
	mean	196.100	26.556	348.129	103.578	413.076	37.204	11.809	0.575	2.454	1.910	2.303	0.358	1.214	0.232	0.065
HD3 (n = 8)	max	177.570	30.150	488.160	118.050	433.760	168.670	12.980	0.980	1.320	3.881	3.582	0.537	1.884	0.321	0.126
	min	113.130	19.970	347.400	106.280	341.690	6.730	8.090	0.230	0.146	1.556	1.575	0.294	0.822	0.174	0.072
	mean	145.939	23.939	389.444	110.488	383.175	36.743	10.006	0.719	0.396	2.356	2.287	0.376	1.243	0.239	0.090
HD4 (n = 8)	max	93.080	242.920	363.950	128.420	92.270	17.470	86.470	1.010	0.390	1.729	2.935	0.495	1.838	0.317	0.115
	min	29.110	132.300	271.960	101.320	64.470	1.930	75.540	0.150	0.049	0.983	1.197	0.250	0.722	0.146	0.034
	mean	62.875	179.826	330.801	116.775	73.861	5.269	79.956	0.549	0.227	1.305	2.014	0.361	1.261	0.230	0.066
C5 (n = 8)	max	6.00	12.26	474.44	34.40	133.43	3.91	336.94	0.32	0.75	2.98	3.76	0.57	2.14	0.33	0.13
	min	0.13	5.02	343.10	25.06	105.78	0.70	244.63	0.00	0.07	0.41	0.60	0.14	0.53	0.15	0.06
	mean	2.58	9.36	408.13	30.61	116.68	2.05	305.03	0.15	0.31	1.75	2.18	0.36	1.25	0.26	0.10
Types	**Statistics**	**Gd**	**Tb**	**Dy**	**Ho**	**Er**	**Tm**	**Yb**	**Lu**	**ϒ**	**ΣREE**	**LREE**	**HREE**	**δEu**	**δCe**	**Y/Ho**
D1 (n = 8)	max	0.15	0.03	0.14	0.03	0.07	0.02	0.08	0.01	0.97	5.86	5.35	0.51	1.01	1.14	51.47
	min	0.07	0.02	0.07	0.02	0.05	0.01	0.01	0.00	0.55	2.56	2.30	0.26	0.68	0.58	23.74
	mean	0.106	0.026	0.093	0.024	0.063	0.012	0.054	0.007	0.763	3.831	3.448	0.383	0.828	0.726	33.211
D2 (n = 8)	max	0.300	0.051	0.243	0.044	0.131	0.018	0.098	0.013	2.321	9.858	9.064	0.814	1.227	0.804	56.718
	min	0.093	0.022	0.085	0.020	0.053	0.007	0.029	0.002	0.971	3.117	2.768	0.349	0.682	0.531	39.538
	mean	0.210	0.037	0.163	0.036	0.090	0.013	0.059	0.009	1.714	6.697	6.082	0.616	0.913	0.695	47.964
HD3 (n = 8)	max	0.354	0.047	0.219	0.041	0.090	0.015	0.042	0.010	2.424	11.143	10.331	0.812	1.753	0.705	65.250
	min	0.171	0.023	0.107	0.024	0.046	0.010	0.014	0.003	1.376	4.994	4.528	0.443	0.944	0.521	49.676
	mean	0.233	0.036	0.153	0.032	0.072	0.012	0.032	0.006	1.854	7.164	6.589	0.575	1.194	0.598	57.916
HD4 (n = 8)	max	0.340	0.056	0.269	0.055	0.136	0.027	0.110	0.019	2.514	8.194	7.287	0.907	1.223	0.878	53.065
	min	0.102	0.021	0.090	0.024	0.058	0.008	0.024	0.002	1.025	3.795	3.439	0.356	0.671	0.531	34.079
	mean	0.209	0.037	0.174	0.039	0.094	0.017	0.065	0.010	1.771	5.882	5.236	0.646	0.912	0.714	45.242
C5 (n = 8)	max	0.43	0.06	0.29	0.06	0.14	0.02	0.10	0.02	3.67	10.78	9.84	1.03	1.56	0.86	72.56
	min	0.18	0.04	0.15	0.04	0.07	0.01	0.02	0.00	2.13	2.46	1.89	0.58	0.63	0.55	42.24
	mean	0.32	0.05	0.20	0.05	0.10	0.01	0.05	0.01	2.77	6.68	5.89	0.79	1.04	0.67	59.26

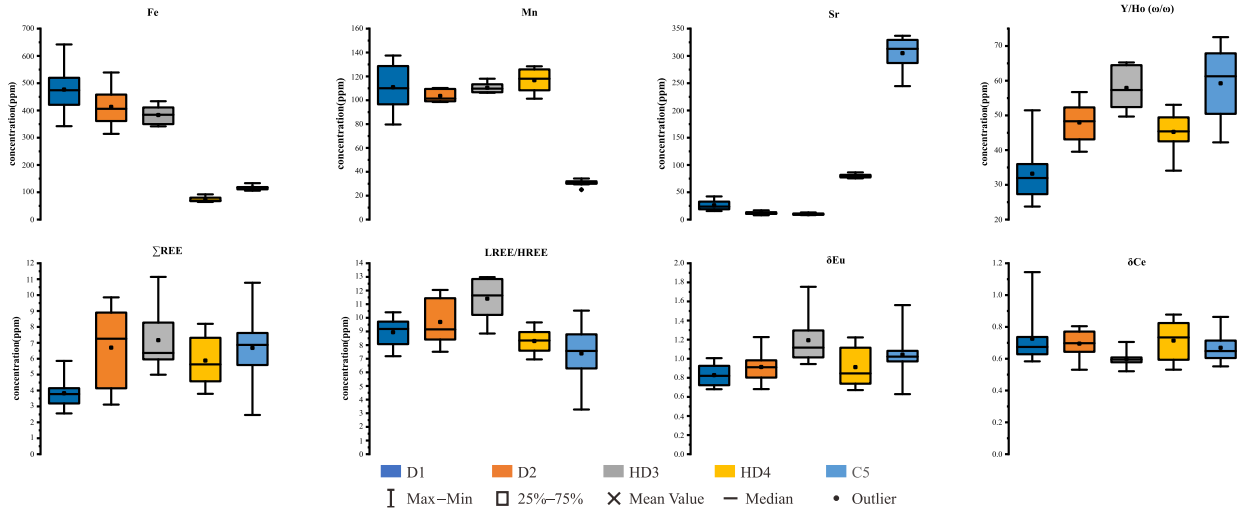

Figure 7. Box diagrams showing the contents of trace elements in dolomite from the Fuli Pb-Zn deposit.

In the early stage of mineralization, the content of Fe in D1 dolomite (n = 8) varied greatly (Figure 7) from 342.28 × 10^{-6} to 642.03 × 10^{-6} (mean value: 476.725 × 10^{-6}). The content of Mn was 79.68 × 10^{-6}–137.45 × 10^{-6} (mean value: 110.95 × 10^{-6}). ΣREE was 2.56 × 10^{-6}–5.86 × 10^{-6} (mean value: 3.83 × 10^{-6}). The ratio of light to heavy rare earth elements (LREE/HREE) was 7.18–10.41 (Mean value: 8.94). The Eu anomaly was insignificant (δEu = 0.68–1.01), and the negative Ce anomaly was strong (δCe = 0.58–1.14, mean value: 0.73, Figure 7). The Y/Ho ratio was 23.74–51.147.

In the early stage of mineralization, the Fe content in D2 dolomite (n = 8) was 314.17 × 10^{-6}–539.23 × 10^{-6} (mean value: 476.73×10^{-6}). The Mn content was 98.52 × 10^{-6}–110.24 × 10^{-6} (mean value: 103.58 × 10^{-6}). ΣREE was 3.117 × 10^{-6}–9.858 × 10^{-6} (mean value: 6.697 × 10^{-6}). LREE/HREE was 7.508–12.042 (mean value: 9.693). The Eu anomaly was insignificant (δEu = 0.682–1.227), and the negative Ce anomaly was strong (δCe = 0.531–0.804, Figure 7). The Y/Ho ratio was 39.54–56.72 (Figure 7).

In the main metallogenic period, the Fe content in HD3 dolomite (n = 8) was 341.69 × 10^{-6}–433.76 × 10^{-6} (mean value: 383.175 × 10^{-6}). The Mn content was 106.28 × 10^{-6}–118.05 × 10^{-6} (mean value: 110.49×10^{-6}). ΣREE was 4.99 × 10^{-6}–11.143 × 10^{-6} (mean value: 7.164 × 10^{-6}). LREE/HREE was 8.85–12.94 (mean value: 11.40). The positive Eu anomaly was weak (δEu = 0.944–1.753, mean value: 1.194), and the negative Ce anomaly was strong (δCe = 0.521–0.705, Figure 7). The Y/Ho ratio was 49.68–65.25.

In the main metallogenic period, the Fe content in HD4 dolomite (n = 8) was 64.47 × 10^{-6}–92.27 × 10^{-6} (mean value: 73.861 × 10^{-6}). The Mn content was 101.32 × 10^{-6}–128.42 × 10^{-6} (mean value: 116.78 × 10^{-6}). ΣREE was 3.79 × 10^{-6}–8.194 × 10^{-6} (mean value: 5.88 × 10^{-6}). LREE/HREE was 6.95–9.66 (mean value: 8.3). The Eu anomaly was insignificant (δEu = 0.67–1.22), and the negative Ce anomaly was weak (δCe = 0.53–0.88, mean value: 0.71, Figure 7). The Y/Ho ratio was 34.08–53.06.

In the late metallogenic period, the Fe content of C5 calcite (n = 8) was 105.78 × 10^{-6}–133.43 × 10^{-6} (Mean value: 116.68 × 10^{-6}). The Mn content was 25.06 × 10^{-6}–34.40 × 10^{-6} (mean value: 30.61 × 10^{-6}). ΣREE was 2.46 × 10^{-6}–10.78 × 10^{-6} (mean value: 6.68 × 10^{-6}). LREE/HREE was 3.27–10.53 (mean value: 7.39). The positive Eu anomaly was weak (δEu = 0.63–1.56, mean value: 1.04), and the negative Ce anomaly was weak (δCe = 0.53–0.88, mean value: 0.71, Figure 7). Y/Ho was 34.08–53.06.

4.3. C-O Isotopic Characteristics

The analytical results of the C-O isotopic compositions are listed in Table 2.

Table 2. C and O isotopic compositions of dolomite in the Fuli Pb-Zn deposit.

Mineral Deposit	Sample No.	Period	$\delta^{13}C_{PDB}$ (‰)	$\delta^{18}O_{SMOW}$ (‰)
Fuli	FL3-6	Wall rock	4.08	19.56
	FL1-6	D1	3.50	20.55
	FL8-2	D1	2.59	16.98
	FL9-I	D1	2.62	17.05
	FL6-4	D2	2.92	16.91
	FL-8-3	HD3	1.97	16.46
	FL3-3	HD3	2.95	16.76
	FL3-1	HD3	2.84	16.33
	FL3-2	HD3	2.82	16.70
	FL14-1	HD3	−4.13	15.02
	FL 4-6	HD4	2.78	16.18
	FL4-2	HD4	3.02	16.64
	FL1-2	HD4	1.08	13.29
	FL6-1	HD4	−2.54	15.51
	FL8-1	HD4	−3.18	14.76
	FLASCAL	C5	−0.85	22.48

The $\delta^{18}O_{SMOW}$ value for the Yangxin Formation dolomite wall rock was 19.56‰, and the $\delta^{13}C_{PDB}$ value was 4.08‰.

In the early metallogenic period, the $\delta^{18}O_{SMOW}$ value for dolomite ranged from 16.91‰ to 20.55‰, with an average value of 17.87‰. The $\delta^{13}C_{PDB}$ value ranged from 2.59 to 3.5‰, with an average value of 2.91‰.

In the main metallogenic period, the $\delta^{18}O_{SMOW}$ value for the dolomite ranged from 13.29‰ to 16.76‰, with an average value of 15.77‰. The $\delta^{13}C_{PDB}$ value ranged from −4.13‰ to 3.02‰, with an average value of 0.76‰.

In the late metallogenic period, the $\delta^{18}O_{SMOW}$ value for calcite was 22.48‰, and the $\delta^{13}C_{PDB}$ value was −0.85‰.

5. Discussion

5.1. Origin of Hydrothermal Dolomite

Y and Ho have been reported to show similar geochemical behaviors in fluid migration [25–28]. Therefore, the Y/Ho ratios can effectively reflect the source of fluid [29,30]. The Y/Ho ratios of different fluids (seawater, brine, etc.) are significantly different. The Y/Ho ratios of deep brines (and unaffected by seawater) tend to be relatively low because these brines might interact with basement strata formations or sediments; the Y/Ho ratios are close to those of the upper crust (27.5) or chondrites (25–28) [31–33]. In this study, the Y/Ho ratios of hydrothermal dolomite found in the different stages of the Fuli Pb-Zn deposits ranged between 33.21 and 72.56 (mean value: 48.72). These Y/Ho ratios are higher than those of typical brines, and some of the ratios are lower than those of marine carbonates. This implies that the fluid that formed the hydrothermal dolomite was mixed with the carbonate wall rock, which is consistent with the overall horizontal distribution of dolomite (rock) on the Y/Ho-La/Ho map (Figure 8). Meanwhile, the distribution of stone (rock) in the Y/Ho-La/Ho diagram shows obvious stratification, implying that the formation of dolomite was affected by the mixing of various fluids.

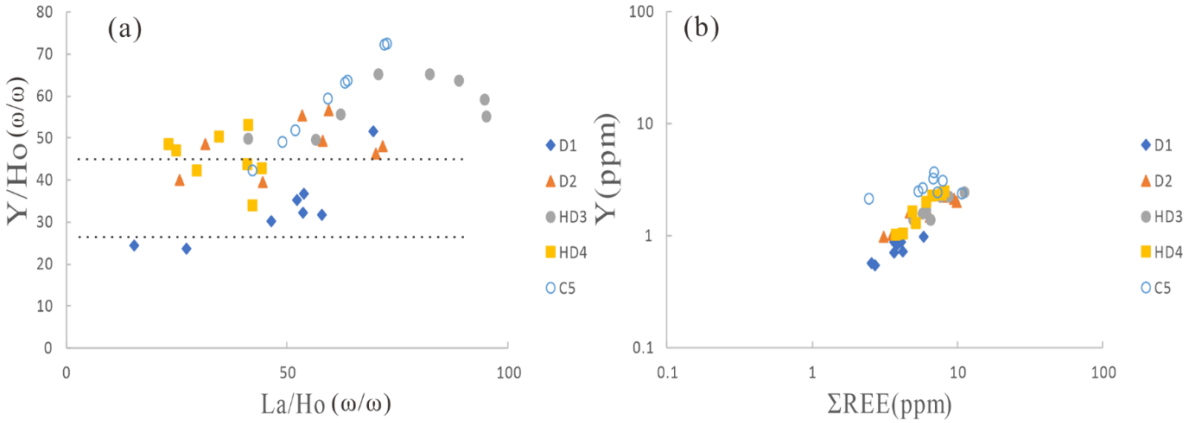

Figure 8. La/Ho vs. Y/Ho (**a**) and Y vs. ∑REE (**b**) diagrams for dolomite from the Fuli Pb-Zn deposit.

5.2. Sources of C and O

The C and O isotopic compositions of hydrothermal dolomite can effectively trace the source of mineralizing materials [6,34,35]. There are three main sources of C and O in a hydrothermal system: (1) the mantle ($\delta^{13}C$ = −8‰ to −4‰, $\delta^{18}O$ = +6‰ to 10‰) [36–38]; (2) marine carbonate rocks ($\delta^{13}C$ = −4‰ to +4‰, $\delta^{18}O$ = +20‰ to +30‰) [39,40]; and (3) sedimentary organic matter ($\delta^{13}C$ = −30‰ to + 10‰, $\delta^{18}O$ = +24‰ to +30‰) [41,42]. As shown in Figure 9, the hydrothermal dolomite of the Fuli deposit is significantly different from the sedimentary organic matter. The $\delta^{13}C_{PDB}$ and $\delta^{18}O_{SMOW}$ values for the wall rocks of the Fuli deposit are slightly smaller than those of the marine carbonate rocks. The C and O isotopic composition range of hydrothermal dolomite is between the values for the primary and marine carbonate rocks; this indicates that the C in the ore-forming fluids of the Fuli deposit might originate from the sedimentary contamination of the mantle multiphase system, effects of high temperature, or the dissolution of marine carbonates. According to the microscopic thermometry of fluid inclusions in the Fuli deposit (Liang, unpublished data), the ore-forming fluids in this area comprised medium- and low-temperature fluids, suggesting that high-temperature differentiation could not be the main factor. In Figure 9, most of the projection points of $\delta^{13}C_{PDB}$ and $\delta^{18}O_{SMOW}$ are distributed nearly horizontally, while only a few suggest the depletion of $\delta^{13}C_{PDB}$ and $\delta^{18}O_{SMOW}$ at the same time. These patterns indicate the influence of dissolution of marine carbonates, while the lower $\delta^{18}O$ could be due to the O isotope exchange between the wall rock and the depleted $\delta^{18}O$ ore-forming fluid.

5.3. Properties of Ore-Forming Fluids

During geological processes, rare earth elements (REEs) have similar geochemical behavior and often migrate as a whole. In addition, as the radii of rare earth ions are similar to those of Ca^{2+} ions, REEs are often concentrated into Ca-bearing mineral lattices via isomorphic substitutions, resulting in negligible rare earth contents in sulfides [43–46]. Therefore, the rare earth compositions of Ca-bearing minerals may reflect the REE-induced characteristics of ore-forming fluids; therefore, the rare earth distribution model has become a reliable tool to explore the source and evolution of ore-forming fluids [47–54].

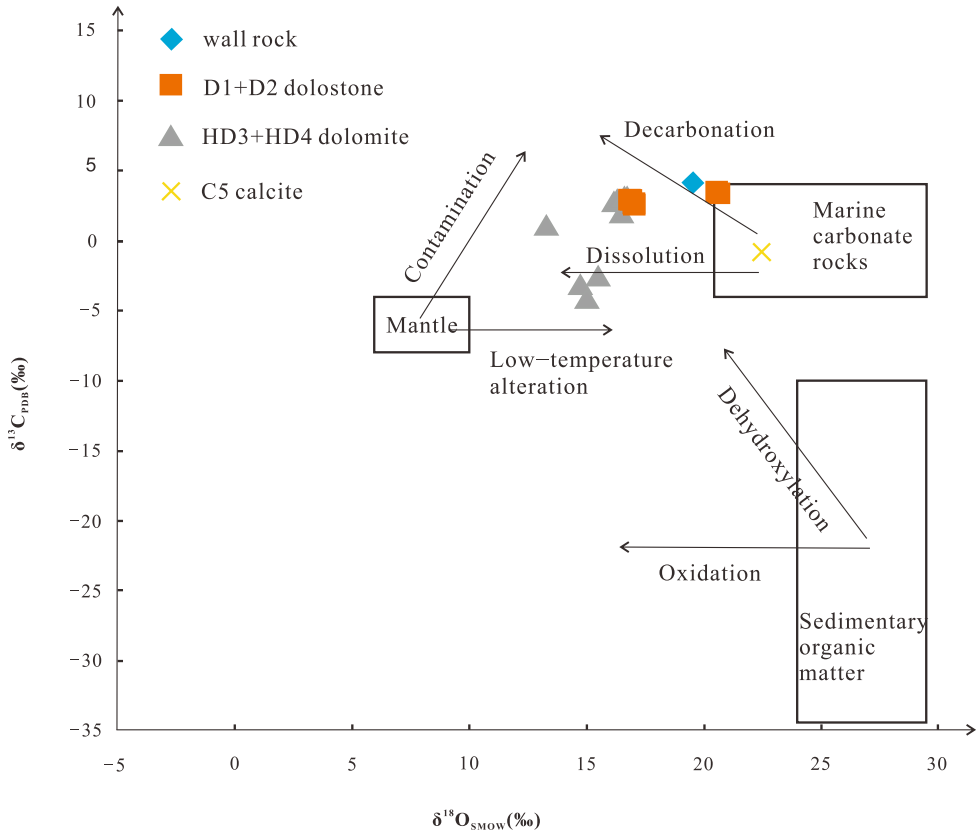

Figure 9. C vs. O isotopic compositions of carbonates from the Fuli Pb-Zn deposit (modified from Zhou et al., 2018).

Eu and Ce anomalies can reflect the redox conditions of ore-forming fluids. Eu has two ionic states in nature: Eu^{3+} and Eu^{2+}. Eu^{3+} has similar properties to other REE trivalent ions. Eu^{2+} is relatively active, and it often enters the Ca^{2+} ion lattices of minerals, leading to positive Eu anomalies [55]. The Eu anomaly is determined by the temperature, pressure, the pH of the ore-forming fluid, and the state of occurrence of the REEs; among these factors, the Eu anomaly is most sensitive to temperature [56]. As demonstrated by Moller et al. [57], at higher temperatures (>200 °C), Eu^{3+} is reduced to Eu^{2+}, which does not readily enter the crystalline structure of minerals; hence, a negative Eu anomaly in carbonate forms in equilibrium with the fluids if the temperature is above 200 °C. Furthermore, preservation of positive Eu anomalies requires that the fluid cools sufficiently to stabilize Eu^{3+}. The ionic radius of Eu^{3+} is 0.99, similar to that of Ca^{2+}; hence, it is easy for Eu^{3+} to displace Ca^{2+} in the mineral lattice, resulting in a positive Eu anomaly [58,59]. The Eu anomalies of D1 and D2 dolomites in the Fuli deposit are insignificant, indicating that the fluids were primarily low in temperature with high oxygen fugacity. The HD3 grey hydrothermal dolomite exhibited a weak positive Eu anomaly (Figure 10), which might be indicative of a gradual decrease in the temperature of the ore-forming fluid with the progress of mineralization. Furthermore, the fluid gradually became enriched in Eu^{2+}. Sulfide precipitation and the formation of hydrothermal dolomite were accompanied by the reduction of Eu^{3+} to Eu^{2+}, indicating that the precipitation of sulfide and dolomite may have resulted from the decreases in oxygen fugacity and temperature of the fluid; the positive Eu anomaly reflects the relatively reducing environment. Ce anomalies are determined by the pH and fO_2 of the ore-forming fluids and are more sensitive to pH [60]. Ce^{3+} is oxidized to Ce^{4+}, which has low solubility and is easily lost from the ore-forming fluid via hydroxide adsorption, resulting in a negative Ce anomaly [61]. The negative Ce anomalies of the D1 and D2 dolomites of the Fuli deposit were significant, and Ce^{4+} adsorbed hydroxide in the ore-forming fluids, indicating that the fluid was alkaline when

the wall rocks were altered by hydrothermal fluids. The HD3 grey hydrothermal dolomite showed a strong negative Ce anomaly, while the HD4 white hydrothermal dolomite and C5 late calcite showed weakly negative Ce anomalies (Figure 10). These patterns indicate that the basicity of the ore-forming environment weakened followed by an evolution of the ore-forming environment to neutrality and finally weak acidity.

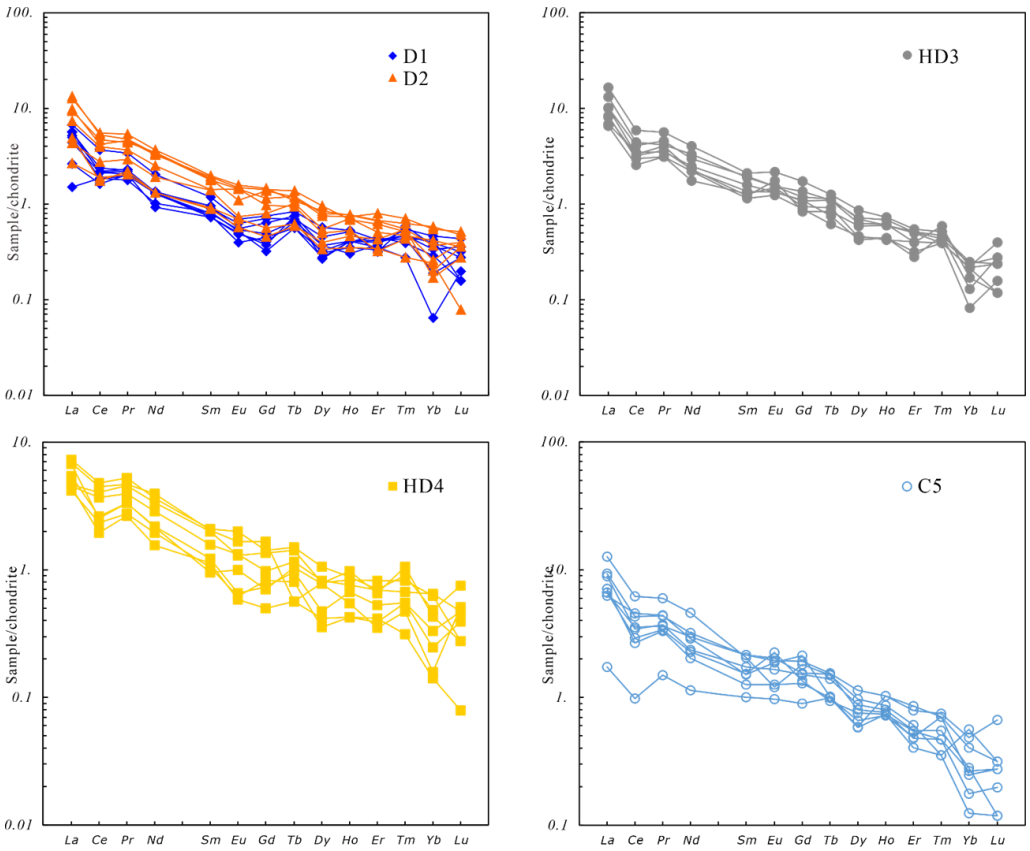

Figure 10. Chondrite-normalized REE patterns of dolomites from the Fuli Pb-Zn deposit (normalization values after Sun & McDonough [62]).

As shown in Figure 11, the D1 and D2 dolomites of the Fuli deposit are enriched in Fe and Mn. Moving from the HD3 grey hydrothermal dolomite to the HD4 white hydrothermal dolomite, Fe and Mn show a downward trend. Fe and Mn entered the carbonate in an alkaline environment, whereas Fe and Mn were released into the fluid in an acidic environment. Thus, as the metasomatism changed from strong to weak, the ore-forming environment predominantly changed from alkaline to acidic. The Sr content increased from D2 dolomite to HD3 grey hydrothermal dolomite, HD4 white hydrothermal dolomite, and late calcite, which might indicate that the continuous reaction between the hydrothermal fluid and the wall rock releases Sr in the wall rock into the fluid. The changes in the Fe, Mn, and Sr contents suggest that mineralization might result from the mixing of the two fluids.

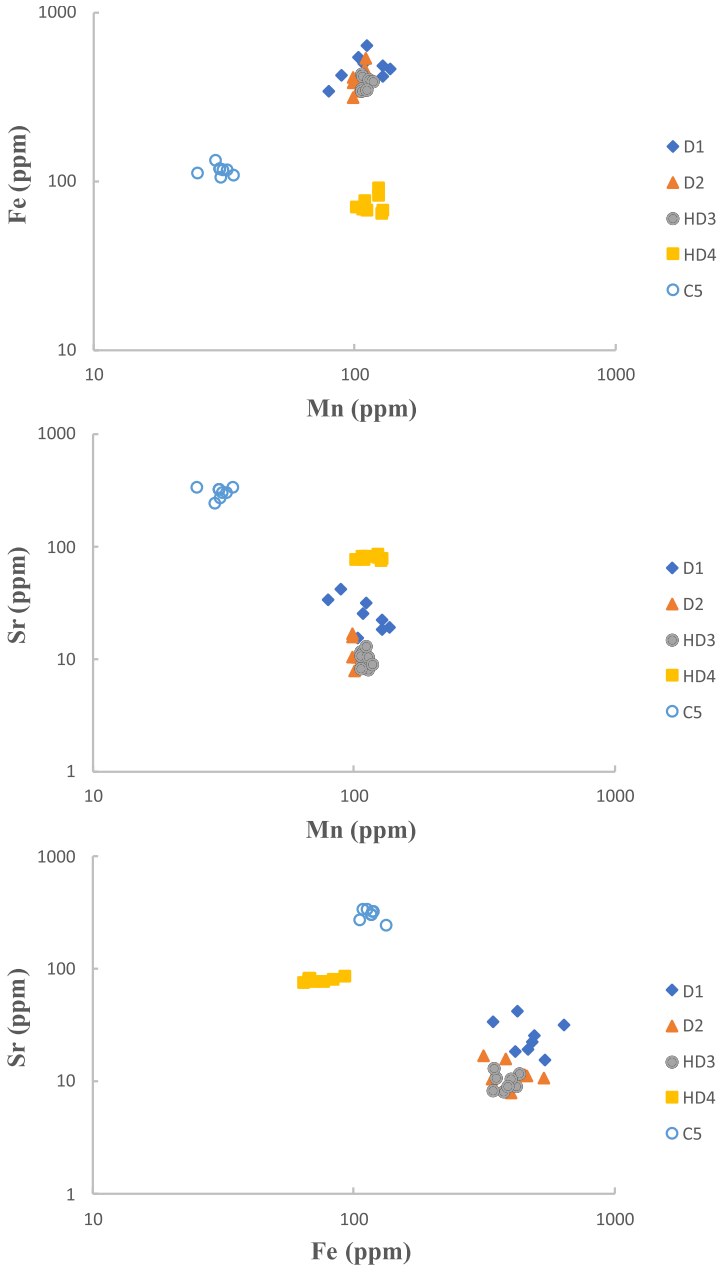

Figure 11. Plots of LA-ICP-MS data from carbonate depicting relative changes in Mn, Fe, and Sr in the Fuli Pb-Zn deposit.

5.4. Ore Genesis Model

There are three mechanisms that may lead to sulfide precipitation: the reduced sulfur mechanism, the sulfate reduction mechanism, and the mixing mechanism. In the reduced sulfur mechanism, that metallogenic metals and reduced sulfur coexist in the same fluid, and sulfides precipitate out due to pH changes, cooling, or dilution of the fluid [58,63–65]. The most critical problem in this model is that the solubility of sulfide in the fluid is considered to be very low; therefore, it is difficult for the fluid to allow the coexistence of a large amount of metal and reduced sulfur. The sulfate reduction mechanism requires that the ore-forming metals are transported to the ore-forming area in the form of sulfate; reduced sulfur is then formed via bacterial reduction or the thermochemical reduction of sulfate. Finally, the reduced sulfur and ore-forming metals react and precipitate out [66–68]. In the mixing mechanism, a fluid transports ore-forming metals, and another fluid transports the reduced sulfur. The mixing of the two fluids results in the precipitation of metal sulfides [37,38,69–74].

The Permian Yangxin Formation is a stratum of limestone mixed with dolomite. The water in this formation is stored between the stratum and remains in balance with calcium carbonate. Limestone mixed with the dolomite stratum contains a large amount of organic matter and pyrite formed during the depositional period; hence, the formation water occurs in an alkaline environment with low oxygen fugacity and low temperature, and it can produce reduced S from the marine sulfates hosted in the regional rocks by the TSR reaction to form a fluid rich in reduced sulfur-bearing. Based on the reduction in oxygen fugacity and temperature of the environment during mineralization along with the evolution from alkaline to neutral to weakly acidic, one can infer that mineralization might be the result of the mixing of the fluid containing metal elements and water in the sedimentary formation. Studies on fluid inclusions in the Fuli deposit (unpublished data) have shown homogeneous temperatures distributions in the fluid inclusions in the sphalerite of the Fuli Pb-Zn deposit, with temperatures between 110 °C and 210 °C. The salinity distribution has two intervals: one between 2% and 11% NaCleqv and a second between 19% and 23% NaCleqv. The ore-forming fluid may be a mixture of medium–low-temperature, and low-salinity fluids with medium–low temperature, and high-salinity fluids.

Integrating all available information, the mineralization model of the Fuli deposit can be described as follows (Figure 12): Thermal activity related to the Indosinian Orogeny resulted in the circulation of hydrothermal fluids within basement rocks (Kunyang Group clastic rocks). These fluids carried up abundant metals and were likely acidic with high oxygen fugacity and high temperature. In the early mineralization stage, compressional tectonics drove the hydrothermal fluids upward along regional faults to the surface, and the wall rocks were subjected to hydrothermal alteration to form D1 and D2 dolomites. During syn-mineralization, the hydrothermal fluids (carrying abundant metals) migrated upwards and mixed with H_2S-rich fluid from the regional strata. This resulted in the precipitation of metallic sulfides and hydrothermal crystalline dolomites in the middle Permian Yangxin Formation, where the faults and contact zones are well developed. In the post-mineralization period, the circulating process between dissolution and re-precipitation in carbonate rocks can cause calcite precipitation [13,75]. Moving from the early stage to the late stage, the oxygen fugacity of the fluid evolved from high to low, and the metallogenic environment changed from alkaline to neutral/weakly acidic. Mineralization occurred due to the changes in the physical and chemical conditions of the ore-forming fluid.

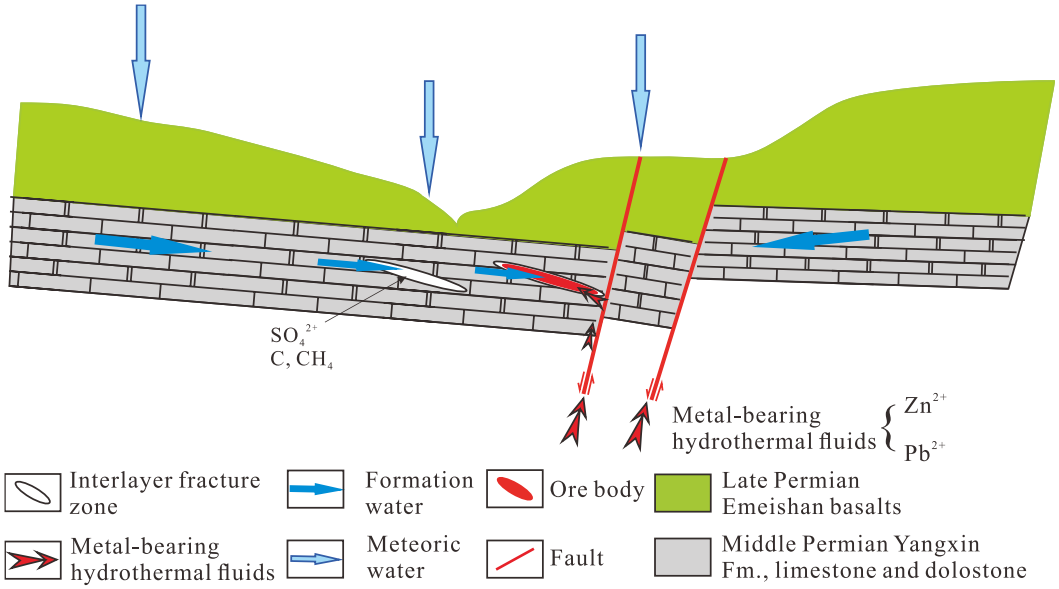

Figure 12. A sketch of the metallogenic model favoured for the Fuli Pb-Zn deposit.

Therefore, we suggest that the Fuli Pb-Zn deposit might have formed due to the mixing of metal-rich, oxidized acidic fluid with sulfur-rich, reduced alkaline fluid.

6. Conclusions

(1) The dolomite from the Fuli deposit exhibits both dark and bright luminescence under CL, with primarily bright luminescence. Moving from early dolomite to late calcite, the luminescence shifts from dark to bright and back to dark.

(2) The C-O isotopic data suggest that the source of C in the Fuli Pb-Zn deposit might be the dissolution of marine carbonates. In contrast, the O isotopic signature is related to the sedimentary rock contamination of the mantle multiphase system, while the relatively low $\delta^{18}O$ might be attributed to O isotope exchange between the wall rock and the depleted $\delta^{18}O$ ore-forming fluid.

(3) For dolomite and calcite in the Fuli Pb-Zn deposit, the insignificant Eu anomaly evolved into a positive Eu anomaly, and the strongly negative Ce anomaly became a weakly negative Ce anomaly. These patterns indicate that the precipitation of sulfide and dolomite was due to the O fugacity of the fluid. Mineralization was also accompanied by a decrease in temperature and change in the fluid environment from alkaline to neutral to weakly acidic.

(4) The Fuli Pb-Zn deposit might have formed due to the mixing of metal-rich,oxidized acidic fluid with sulfur-rich, reduced alkaline fluid.

(5) A combination of the characteristics of stratum control and epigenetic ore-forming of the Fuli Pb-Zn deposit suggests that the Fuli Pb-Zn deposit is an MVT deposit.

Author Contributions: Formal analysis, X.Z.; Investigation, C.Z., H.Q. and G.L.; Writing—original draft, X.L.; Writing—review & editing, B.L. All authors have read and agreed to the published version of the manuscript.

Funding: This research received no external funding.

Institutional Review Board Statement: Not applicable.

Informed Consent Statement: Not applicable.

Data Availability Statement: Not applicable.

Conflicts of Interest: The authors declare no conflict of interest.

References

1. Liu, H.C. Emeishan Basalt and Pb-Zn Metallogenesis. *Geol. Explor.* **1995**, *31*, 1–6.
2. Huang, Z.L.; Chen, J.; Han, R.S.; Li, W.B.; Liu, C.Q.; Zhang, Z.L.; Ma, D.Y.; Gao, D.R.; Yang, H.L. *Geochemistry and Ore-Formation of the Huize Giant Lead-Zinc Deposit, Yunnan Province, China: Discussion on the Relationship between Emeishan Flood Basalts and Lead-zinc Mineralization*; Geological Publishing House: Beijing, China, 2004.
3. Huang, Z.L.; Zhong, H.U.R.; Shu, W.; Wen, H.; Liu, S.; Fu, Y. A Study on the Large-Scale Low-Temperature Metallogenic Domain in Southwestern China—Significance, History and New Progress. *Acta Mineral. Sin.* **2011**, *31*, 309–314.
4. Hu, R.U.; Zhou, M.E. Multiple Mesozoic Mineralization Events in South China—An Introduction to the Thematic Issue. *Miner. Depos.* **2012**, *47*, 579–588. [CrossRef]
5. Hu, R.; Fu, S.; Huang, Y.; Zhou, M.F.; Fu, S.; Zhao, C.; Wang, Y.; Bi, X.; Xiao, J. The Giant South China Mesozoic Low-Temperature Metallogenic Domain: Reviews and a New Geodynamic Model. *J. Asian Earth Sci.* **2017**, *137*, 9–34. [CrossRef]
6. Zhou, J.X.; Xiang, Z.Z.; Zhou, M.F.; Feng, Y.X.; Luo, K.; Huang, Z.L.; Wu, T. The Giant Upper Yangtze Pb–Zn Province in SW China: Reviews, New Advances and a New Genetic Model. *J. Asian Earth Sci.* **2018**, *154*, 280–315. [CrossRef]
7. Liu, H.C.; Lin, W.D. *Regularity Research of Ag, Zn, Pb Ore Deposits North-East Yunnan Province*; Yunnan University Press: Kunming, China, 1999.
8. Ore-forming model of Huize rich Pb-Zn deposit, Yunnan. *Acta Mineral. Sin.* **2001**, *21*, 674–680. Available online: https://www.researchgate.net/publication/286785197_Ore-forming_model_of_Huize_rich_Pb-Zn_deposit_Yunnan (accessed on 22 May 2022).
9. Han, R.S.; Liu, C.Q.; Huang, Z.L.; Chen, J.; Ma, D.Y.; Li, Y. Genesis Modeling of Huize Lead-Zinc Ore Deposit in Yunnan. *Acta Mineral. Sin.* **2001**, *21*, 674–680.
10. Xu, Y.; Huang, Z.; Zhu, D.; Luo, T. Origin of Hydrothermal Deposits Related to the Emeishan Magmatism. *Ore Geol. Rev.* **2014**, *63*, 1–8. [CrossRef]
11. Zhou, J.-X.; Huang, Z.L.; Zhou, M.-F.; Zhu, X.-K.; Muchez, P. Zinc, Sulfur and Lead Isotopic Variations in Carbonate-Hosted Pb–Zn Sulfide Deposits, Southwest China. *Ore Geol. Rev.* **2014**, *58*, 41–54. [CrossRef]

12. Zhou, J.X.; Bai, J.H.; Huang, Z.L.; Zhu, D.; Yan, Z.F.; Lv, Z.C. Geology, Isotope Geochemistry and Geochronology of the Jinshachang Carbonate-Hosted Pb–Zn Deposit, Southwest China. *J. Asian Earth Sci.* **2015**, *98*, 272–284. [CrossRef]
13. Zhou, J.X.; Luo, K.; Wang, X.C.; Wilde, S.A.; Wu, T.; Huang, Z.L.; Cui, Y.L.; Zhao, J.X. Ore Genesis of the Fule Pb Zn Deposit and Its Relationship with the Emeishan Large Igneous Province: Evidence from Mineralogy, Bulk COS and in Situ SPb Isotopes. *Gondwana Res.* **2018**, *54*, 161–179. [CrossRef]
14. Jin, Z.G.; Zhou, J.X.; Huang, Z.L.; Luo, K.; Gao, J.G.; Peng, S.; Wang, B.; Chen, X.L. Ore genesis of the Nayongzhi Pb-Zn deposit, Puding City, Guizhou Province, China: Evidences from S and in situ Pb isotopes. *Acta Petrol. Sin.* **2016**, *32*, 3441–3455.
15. Li, Z.L. Geological Geochemical Characteristics and Prospecting Directions in the Fule Lead-Zinc Deposit, Yunnan Province. Master's Thesis, University of Chinese Academy of Sciences, Beijing, China, 2016.
16. Cui, Y.L.; Zhou, J.X.; Huang, Z.L.; Luo, K.; Nian, H.L.; Lin, Y.; Li, Z.L. Geology, geochemistry and ore genesis of the Fule Pb-Zn deposit, Yunnan Province, Southwest China. *Acta Petrol. Sin.* **2018**, *34*, 194–206.
17. Leach, D.L.; Sangster, D.F.; Kelley, K.D.; Large, R.R.; Garven, G.; Allen, C.R.; Gutzmer, J.; Walters, S. Sediment-Hosted Lead-Zinc Deposits: A Global Perspective. In *Economic Geology*; Society of Economic Geologists: Littleton, CO, USA, 2005; Volume 100, pp. 561–607.
18. Peng, J.; Zhang, D.L.; Hu, R.Z.; Wu, M.J.; Liu, X.M.; Qi, L.; Yu, Y.L. Inhomogeneous Distribution of Rare Earth Elements (Rees) in Scheelite from the Zhazixi w-Sb Deposit, Western Hunan and Its Geological Implications. *Geol. Rev.* **2010**, *56*, 810–819.
19. Heinrich, C.A.; Pettke, T.; Halter, W.E.; Aigner-Torres, M.; Audétat, A.; Günther, D.; Hattendorf, B.; Bleiner, D.; Guillong, M.; Horn, I. Quantitative Multi-Element Analysis of Minerals, Fluid and Melt Inclusions by Laser-Ablation Inductively-Coupled-Plasma Mass-Spectrometry. *Geochim. Cosmochim. Acta* **2003**, *67*, 3473–3497. [CrossRef]
20. Lyu, C.; Gao, J.F.; Qi, L.; Huang, X.W. Re-Os Isotope System of Sulfide from the Fule Carbonate-Hosted Pb-Zn Deposit, SW China: Implications for Re-Os Dating of Pb-Zn Mineralization. *Ore Geol. Rev.* **2020**, *121*, 103558. [CrossRef]
21. Zong, K.; Klemd, R.; Yuan, Y.; He, Z.; Guo, J.; Shi, X.; Liu, Y.; Hu, Z.; Zhang, Z. The Assembly of Rodinia: The Correlation of Early Neoproterozoic (ca. 900 Ma) High-Grade Metamorphism and Continental Arc Formation in the Southern Beishan Orogen, Southern Central Asian Orogenic Belt (CAOB). *Precambrian Res.* **2017**, *290*, 32–48. [CrossRef]
22. Hu, Z.; Zhang, W.; Liu, Y.; Gao, S.; Li, M.; Zong, K.; Chen, H.; Hu, S. "Wave" Signal-Smoothing and Mercury-Removing Device for Laser Ablation Quadrupole and Multiple Collector ICPMS Analysis: Application to Lead Isotope Analysis. *Anal. Chem.* **2014**, *87*, 1152–1157. [CrossRef]
23. Liu, Y.; Hu, Z.; Gao, S.; Günther, D.; Xu, J.; Gao, C.; Chen, H. In Situ Analysis of Major and Trace Elements of Anhydrous Minerals by LA-ICP-MS without Applying an Internal Standard. *Chem. Geol.* **2008**, *257*, 34–43. [CrossRef]
24. Chen, L.; Liu, Y.; Hu, Z.; Gao, S.; Zong, K.; Chen, H. Accurate Determinations of Fifty-Four Major and Trace Elements in Carbonate by LA–ICP-MS Using Normalization Strategy of Bulk Components as 100%. *Chem. Geol.* **2011**, *284*, 283–295. [CrossRef]
25. Bau, M.; Dulski, P. Comparative Study of Yttrium and Rare-Earth Element Behaviours in Fluorine-Rich Hydrothermal Fluids. *Contrib. Mineral. Petrol.* **1995**, *119*, 213–223. [CrossRef]
26. Bau, M. Controls on the Fractionation of Isovalent Trace Elements in Magmatic and Aqueous Systems: Evidence from Y/Ho, Zr/Hf, and Lanthanide Tetrad Effect. *Contrib. Mineral. Petrol.* **1996**, *123*, 323–333. [CrossRef]
27. Bau, M.; Dulski, P. Comparing Yttrium and Rare Earths in Hydrothermal Fluids from the Mid-Atlantic Ridge: Implications for Y and REE Behaviour during near-Vent Mixing and for the Y/Ho Ratio of Proterozoic Seawater. *Chem. Geol.* **1999**, *155*, 77–90. [CrossRef]
28. Cherniak, D.J.; Zhang, X.Y.; Wayne, N.K.; Watson, E.B. Sr, Y, and REE Diffusion in Fluorite. *Chem. Geol.* **2001**, *181*, 99–111. [CrossRef]
29. Wang, Y.; Yang, H.; Liu, C.; Cai, Y.; Tan, J.; Qiu, X.; Zhang, L.; Zhu, S. Lab Strontium and Sulfur Isotopic Characteristics of the Tangjiazhai Pb-Zn Deposit in Western Hunan Province, China: Denotative Significance for Ore-Forming Materials Source. *Geol. China* **2018**, *45*, 564–572.
30. Wang, Q.; Tong, H.; Huang, C.-Y.; Chen, D. Tracing Fluid Sources and Formation Conditions of Miocene Hydrocarbon-Seep Carbonates in the Central Western Foothills, Central Taiwan. *J. Asian Earth Sci.* **2018**, *168*, 186–196. [CrossRef]
31. Nozaki, Y.; Zhang, J.; Amakawa, H. The Fractionation between Y and Ho in the Marine Environment. *Earth Planet. Sci. Lett.* **1997**, *148*, 329–340. [CrossRef]
32. Kamber, B.S.; Greig, A.; Collerson, K.D. A New Estimate for the Composition of Weathered Young Upper Continental Crust from Alluvial Sediments, Queensland, Australia. *Geochim. Cosmochim. Acta* **2005**, *69*, 1041–1058. [CrossRef]
33. Jakubowicz, M.; Dopieralska, J.; Belka, Z. Tracing the Composition and Origin of Fluids at an Ancient Hydrocarbon Seep (Hollard Mound, Middle Devonian, Morocco): A Nd, REE and Stable Isotope Study. *Geochim. Cosmochim. Acta* **2015**, *156*, 50–74. [CrossRef]
34. Zhou, J.; Huang, Z.; Zhou, M.; Li, X.; Jin, Z. Constraints of C–O–S–Pb Isotope Compositions and Rb–Sr Isotopic Age on the Origin of the Tianqiao Carbonate-Hosted Pb–Zn Deposit, SW China. *Ore Geol. Rev.* **2013**, *53*, 77–92. [CrossRef]
35. Zhou, J.X.; Wang, X.C.; Wilde, S.A.; Luo, K.; Huang, Z.L.; Wu, T.; Jin, Z.G. New Insights into the Metallogeny of MVT Zn-Pb Deposits: A Case Study from the Nayongzhi in South China, Using Field Data, Fluid Compositions, and in Situ S-Pb Isotopes. *Am. Mineral.* **2018**, *103*, 91–108. [CrossRef]
36. Taylor, H.P.; Frechen, J.; Degens, E.T. Oxygen and Carbon Isotope Studies of Carbonatites from the Laacher See District, West Germany and the Alnö District, Sweden. *Geochim. Cosmochim. Acta* **1967**, *31*, 407–430. [CrossRef]

37. Grandia, F.; Cardellach, E.; Canals, A.; Banks, D.A. Geochemistry of the Fluids Related to Epigenetic Carbonate-Hosted Zn-Pb Deposits in the Maestrat Basin, Eastern Spain: Fluid Inclusion and Isotope (Cl, C, O, S, Sr) Evidence. *Econ. Geol.* **2003**, *98*, 933–954. [CrossRef]
38. Grandia, F.; Canals, A.; Cardellach, E.; Banks, D.A.; Perona, J. Origin of Ore-Forming Brines in Sediment-Hosted Zn-Pb Deposits of the Basque-Cantabrian Basin, Northern Spain. *Econ. Geol.* **2003**, *98*, 1397–1411. [CrossRef]
39. Veizer, J.; Hoefs, J. The Nature of O18/O16 and C13/C12 Secular Trends in Sedimentary Carbonate Rocks. *Geochim. Cosmochim. Acta* **1976**, *40*, 1387–1395. [CrossRef]
40. Spangenberg, J.; Fontboté, L.; Sharp, Z.D.; Hunziker, J. Carbon and Oxygen Isotope Study of Hydrothermal Carbonates in the Zinc-Lead Deposits of the San Vicente District, Central Peru: A Quantitative Modeling on Mixing Processes and CO_2 Degassing. *Chem. Geol.* **1996**, *133*, 289–315. [CrossRef]
41. Liu, J.M.; Liu, J.J. Basin fluid genetic model of sediment-hosted micro-disseminated gold deposits in the gold-triangle area between Guizhou, Guangxi and Yunnan. *Acta Mineral. Sin.* **1997**, *17*, 448–456.
42. Kump, L.R.; Arthur, M.A. Interpreting Carbon-Isotope Excursions: Carbonates and Organic Matter. *Chem. Geol.* **1999**, *161*, 181–198. [CrossRef]
43. Bau, M. Rare-Earth Element Mobility during Hydrothermal and Metamorphic Fluid-Rock Interaction and the Significance of the Oxidation State of Europium. *Chem. Geol.* **1991**, *93*, 219–230. [CrossRef]
44. Bau, M.; Moeller, P. Rare Earth Elements Fractionation in Metamorphogenic Hydrothermal Calcite, Magnesite and Siderite. *Mineral. Petrol.* **1992**, *45*, 231–246. [CrossRef]
45. Wenbo, L.; Zhilong, H.; Liang, Q. REE Geochemistry of Sulfides from the Huize Zn-Pb Ore Field, Yunnan Province: Implication for the Sources of Ore-Forming Metals. *Acta Geol. Sin.-Engl. Ed.* **2007**, *81*, 442–449. [CrossRef]
46. Tang, Y.Y.; Bi, X.W.; He, L.P.; Wu, L.Y.; Feng, C.X.; Zou, Z.C.; Tao, Y.; Hu, R.Z. Geochemical Characteristics of Trace Elements, Fluid Inclusions and Carbon-Oxygen Isotopes of Calcites in the Jinding Zn-Pb Deposit, Lanping, China. *Acta Petrol. Sin.* **2011**, *27*, 2635–2645.
47. Michard, A. Rare Earth Element Systematics in Hydrothermal Fluids. *Geochim. Cosmochim. Acta* **1989**, *53*, 745–750. [CrossRef]
48. Bau, M.; Romer, R.L.; Lüders, V.; Dulski, P. Tracing Element Sources of Hydrothermal Mineral Deposits: REE and Y Distribution and Sr-Nd-Pb Isotopes in Fluorite from MVT Deposits in the Pennine Orefield, England. *Miner. Depos.* **2003**, *38*, 992–1008. [CrossRef]
49. Zhong, S.; Mucci, A. Partitioning of Rare Earth Elements (REEs) between Calcite and Seawater Solutions at 25 °C and 1 Atm, and High Dissolved REE Concentrations. *Geochim. Cosmochim. Acta* **1995**, *59*, 443–453. [CrossRef]
50. Johannesson, K.H.; Stetzenbach, K.J.; Hodge, V.F. Hodge Rare Earth Elements as Geochemical Tracers of Regional Groundwater Mixing. *Geochim. Cosmochim. Acta* **1997**, *61*, 3605–3618. [CrossRef]
51. Huang, Z.L.; Li, W.; Jin, C.; Jing, W.; Han, R.; Liu, C. REE Geochemistry of Calcites from Fault Zone of Huize Superlarge Pb-Zn Deposits in Yunnan Province. *Miner. Depos.* **2003**, *22*, 199–207.
52. Debruyne, D.; Hulsbosch, N.; Muchez, P. Unraveling Rare Earth Element Signatures in Hydrothermal Carbonate Minerals Using a Source–Sink System. *Ore Geol. Rev.* **2016**, *72*, 232–252. [CrossRef]
53. Liu, G.; Yuan, F.; Deng, Y.; Wang, F.; White, N.C.; Huizenga, J.M.; Li, Y.; Li, X.; Zhou, T. Ore-Fluid Geochemistry of the Hehuashan Pb–Zn Deposit in the Tongling Ore District, Anhui Province, China: Evidence from REE and C–H–O Isotopes of Calcite. *Ore Geol. Rev.* **2020**, *117*, 103279. [CrossRef]
54. Hu, Y.S.; Ye, L.; Wei, C.; Huang, Z.L.; Wang, H.Y. REE Geochemistry of the Hydrothermal Calcites from the Huayuan Orefield, in the Western Hunan, China. *Acta Mineral. Sin.* **2020**, *40*, 441–449.
55. Wang, Z.G.; Yu, X.Y.; Zhao, Z.H. *Rare Earth Element Geochemistry*; Science Press: Beijing, China, 1989.
56. Lüders, V.; Mller, P.; Dulski, P. REE Fractionation in Carbonates and Fluorite. In *Formation of Hydrothermal Vein Deposits: A case study of the Pb-Zn-, barite and fluorite deposits of 1993*; Gebrüder Borntraeger: Stuttgart, Germany, 1993; Volume 30, pp. 133–150.
57. Möller, P.; Bau, M.; Dulski, P.; Lüders, V. REE and Yttrium Fractionation in Fluorite and Their Bearing on Fluorite Formation. In Proceedings of the Ninth Quadrennial IAGOD Symposium, Beijing, China, 12–18 August 1998; pp. 575–592.
58. Sverjensky, D.A. Europium Redox Equilibria in Aqueous Solution. *Earth Planet. Sci. Lett.* **1984**, *67*, 70–78. [CrossRef]
59. Wood, S.A. The Aqueous Geochemistry of the Rare-Earth Elements and Yttrium. *Chem. Geol.* **1990**, *82*, 159–186. [CrossRef]
60. Elderfield, H.; Sholkovitz, E.R. Rare Earth Elements in the Pore Waters of Reducing Nearshore Sediments. *Earth Planet. Sci. Lett.* **1987**, *82*, 280–288. [CrossRef]
61. Lottermoser, B.G. Rare Earth Elements and Hydrothermal Ore Formation Processes. *Ore Geol. Rev.* **1992**, *7*, 25–41. [CrossRef]
62. McDonough, W.F.; Sun, S.-S. The Composition of the Earth. *Chem. Geol.* **1995**, *120*, 223–253. [CrossRef]
63. Anderson, G. Precipitation of Mississippi Valley-Type Ores. *Econ. Geol.* **1975**, *70*, 937–942. [CrossRef]
64. Spirakis, C.S.; Heyl, A.V. Evaluation of Proposed Precipitation Mechanisms for Mississippi Valley-Type Deposits. *Ore Geol. Rev.* **1995**, *10*, 1–17. [CrossRef]
65. Liu, Y.C.; Hou, Z.Q.; Yang, Z.S.; Tian, S.H.; Song, Y.C.; Yang, Z.M.; Wang, Z.L.; Zheng, L.I. Some Insights and Advances in Study of Mississippi Valley-Type(MVT) Lead-Zinc Deposits. *Miner. Depos.* **2008**, *27*, 253–264.
66. Machel, H.G. Bacterial and Thermochemical Sulfate Reduction in Diagenetic Settings—Old and New Insights. *Sedim. Geol.* **2001**, *140*, 143–175. [CrossRef]

67. Anderson, G.M.; Thom, J. The Role of Thermochemical Sulfate Reduction in the Origin of Mississippi Valley-Type Deposits. II. Carbonate–Sulfide Relationships. *Geofluids* **2007**, *8*, 27–34. [CrossRef]
68. Thom, J.; Anderson, G.M. The Role of Thermochemical Sulfate Reduction in the Origin of Mississippi Valley-Type Deposits. I. Experimental Results. *Geofluids* **2007**, *8*, 16–26. [CrossRef]
69. Anderson, G.M. *Some Geochemical Aspects of Sulfide Precipitation in Carbonate Rocks*; James Cook University of North Queensland: Townsville, Australia, 1983.
70. Taylor, M.; Kesler, S.E.; Cloke, P.L.; Kelly, W.C. Fluid Inclusion Evidence for Fluid Mixing, Mascot-Jefferson City Zinc District, Tennessee. *Econ. Geol.* **1983**, *78*, 1425–1439. [CrossRef]
71. Plumlee, G.S.; Leach, D.L.; Hofstra, A.H.; Landis, G.P.; Rowan, E.L.; Viets, J.G. Chemical Reaction Path Modeling of Ore Deposition in Mississippi Valley-Type Pb-Zn Deposits of the Ozark Region, U.S. Midcontinent. *Econ. Geol.* **1994**, *89*, 1361–1383. [CrossRef]
72. Gleeson, S.A.; Turner, W.A. Fluid Inclusion Constraints on the Origin of the Brines Responsible for Pb-Zn Mineralization at Pine Point and Coarse Non-Saddle and Saddle Dolomite Formation in Southern Northwest Territories. *Geofluids* **2007**, *7*, 51–68. [CrossRef]
73. Pfaff, K.; Hildebrandt, L.H.; Leach, D.L.; Jacob, D.E.; Markl, G. Formation of the Wiesloch Mississippi Valley-Type Zn-Pb-Ag Deposit in the Extensional Setting of the Upper Rhinegraben, SW Germany. *Miner. Depos.* **2010**, *45*, 647–666. [CrossRef]
74. Corbella, M.; Ayora, C.; Cardellach, E. Hydrothermal Mixing, Carbonate Dissolution and Sulfide Precipitation in Mississippi Valley-Type Deposits. *Miner. Depos.* **2004**, *39*, 344–357. [CrossRef]
75. Shelton, K.L.; Gregg, J.M.; Johnson, A.W. Replacement Dolomites and Ore Sulfides as Recorders of Multiple Fluids and Fluid Sources in the Southeast Missouri Mississippi Valley-Type District: Halogen-87Sr/86Sr-18O-34S Systematics in the Bonneterre Dolomite. *Econ. Geol.* **2009**, *104*, 733–748. [CrossRef]